Future Journal of Pharmaceutical Sciences

RESEARCH

Open Access

Size-dependent effects of niosomes on the penetration of methotrexate in skin layers

Sakshi Soni[1], Kalpana Baghel[2], Murari Lal Soni[3], Sushil K. Kashaw[1] and Vandana Soni[1*]

Abstract

Background Niosomes hold promise as drug delivery systems for cancer treatment, with niosome size impacting stability, biodistribution, and effectiveness. This study optimized methotrexate (MTX)-loaded niosome formulation by studying the effects of components and processing conditions on size. The niosomes formulation was made by the thin-film hydration technique.

Results The optimized formulation (NIO 17) with a 6:2:2 ratio of span 60, soya PC, and cholesterol achieved 55.05% methotrexate encapsulation, particle size 597.2 nm, PDI 0.49, and zeta potential − 23.3 mV. The compatibility of methotrexate with lipids was confirmed via Fourier transform infrared spectroscopy, and transmission electron microscopy revealed spherical, well-dispersed vesicles. Differential scanning calorimetry indicated methotrexate conversion or entrapment within vesicles. In vitro release exhibited a sustained pattern with an initial burst. NIO 17 showed potent anti-cancer activity against B16-F10 cells (GI50: 38.7176 µg/mL). Ex vivo studies suggest tailoring niosome size (597.2–982.3 nm) to target specific skin depths (0–38 µm) for enhanced localized drug delivery.

Conclusions This study demonstrates the potential of methotrexate-loaded niosomes as a novel cancer therapy approach, highlighting the potent anti-cancer activity and transdermal delivery potential of NIO 17. Further research is necessary to explore its clinical translation.

Keywords Niosomes, Rhodamine B, Confocal microscopy, B16-F10 cell lines, Penetration study

*Correspondence:
Vandana Soni
drsonivandana@gmail.com
Full list of author information is available at the end of the article

Graphical abstract

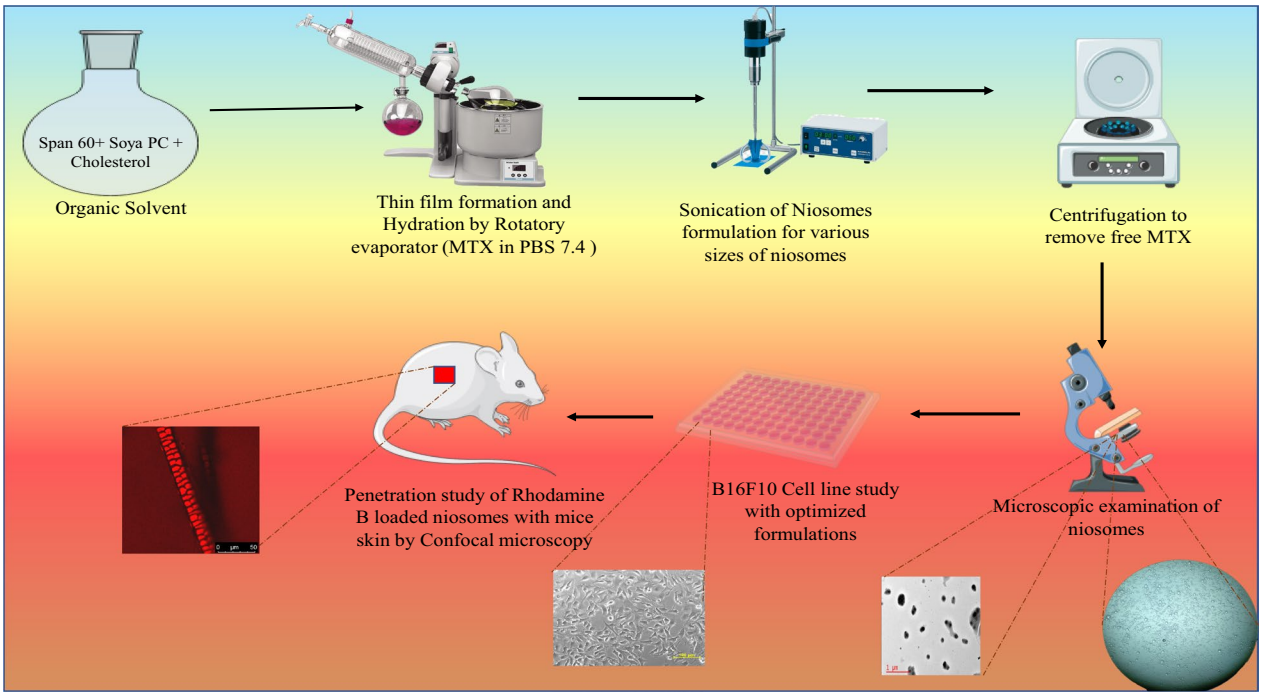

Background

Skin cancer, triggered by ultraviolet (UV) radiation from the sun or tanning beds, affects millions globally [1, 3]. Common types include basal cell carcinoma, squamous cell carcinoma, and melanoma as shown in Fig. 1. Traditional treatments like surgery, radiation therapy, and chemotherapy pose various limitations [2, 3]. Surgery, while common for early stages, is invasive. Radiation uses high-energy beams, and chemotherapy, despite killing cancer cells, often comes with side effects like

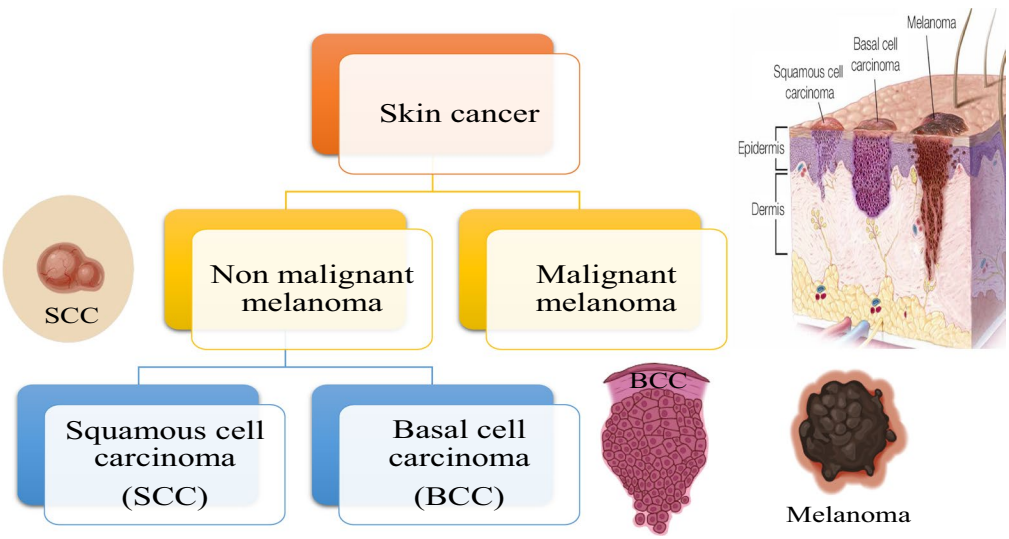

Fig. 1 Schematic representation of SCC, BCC and malignant melanoma

nausea, vomiting, hair loss, and fatigue [4, 6]. Moreover, advanced or metastatic cases often lack effective treatment options. There is a growing demand for targeted and minimally invasive therapies that can deliver drugs specifically to cancerous cells while sparing healthy tissue. In this context, exploring novel drug delivery systems like niosomes holds great promise. Niosomes, with their ability to encapsulate drugs and deliver them to specific sites within the body, offer the potential to enhance the efficacy of treatments for skin cancer while minimizing adverse effects, thus addressing critical unmet needs in the current treatment landscape. Niosomes, composed of biocompatible and biodegradable phospholipids, cholesterol, and surfactants [5, 7], niosomes can deliver a wide range of drugs and target specific cells or tissues. Studies in mice suggest their safety and efficacy for skin cancer treatment, warranting further exploration for clinical use.

Methotrexate (MTX), a drug commonly used for rapidly growing tumors like skin cancer [5], works by hindering DNA synthesis in dividing cells. While traditionally administered orally or parenterally for skin cancer, MTX can cause gastrointestinal side effects like indigestion, dyspepsia, vomiting, and ulceration. To address these, we investigated the potential of niosomes as a topical delivery system for MTX [7].

This study aimed to evaluate niosomes as a means to enhance the transdermal transport of MTX to various skin layers, focusing on the impact of niosome size on their efficacy as shown in Fig. 2. We examined the effects of different-sized niosomes on MTX permeation through ex vivo studies and visualized their distribution within the skin using confocal laser scanning microscopy. Additionally, in vivo histopathological studies in mice assessed the feasibility of using niosomes to deliver MTX to the skin.

Materials and protocols

Chemicals

This research utilized a diverse range of materials for its experiments. The drug, methotrexate (MTX), was kindly provided by Neon Laboratories Ltd. (Mumbai, India). Soya Phosphatidylcholine (SPC), a key lipid component, was a generous gift from Lipoid GmbH (Ludwigshafen, Germany), while cholesterol (CHOL) was purchased from CDH (India). Solvents and reagents like chloroform, methanol, phosphate buffer, Triton X-100, Sephadex G-50, and dimethyl sulfoxide (DMSO) were sourced from HiMedia Laboratory Pvt. Ltd. (Mumbai, India). Additionally, HPLC water (Lichrosolv), acetonitrile (HPLC grade), methanol (HPLC grade), and rhodamine B (RHB) were procured from Sigma-Aldrich and Merck (India). Finally, dialysis bags with molecular weights ranging from 12,000 to 14,000 were obtained from HiMedia Laboratory Pvt. Ltd. Notably, all chemicals were of analytical grade and used directly without further purification.

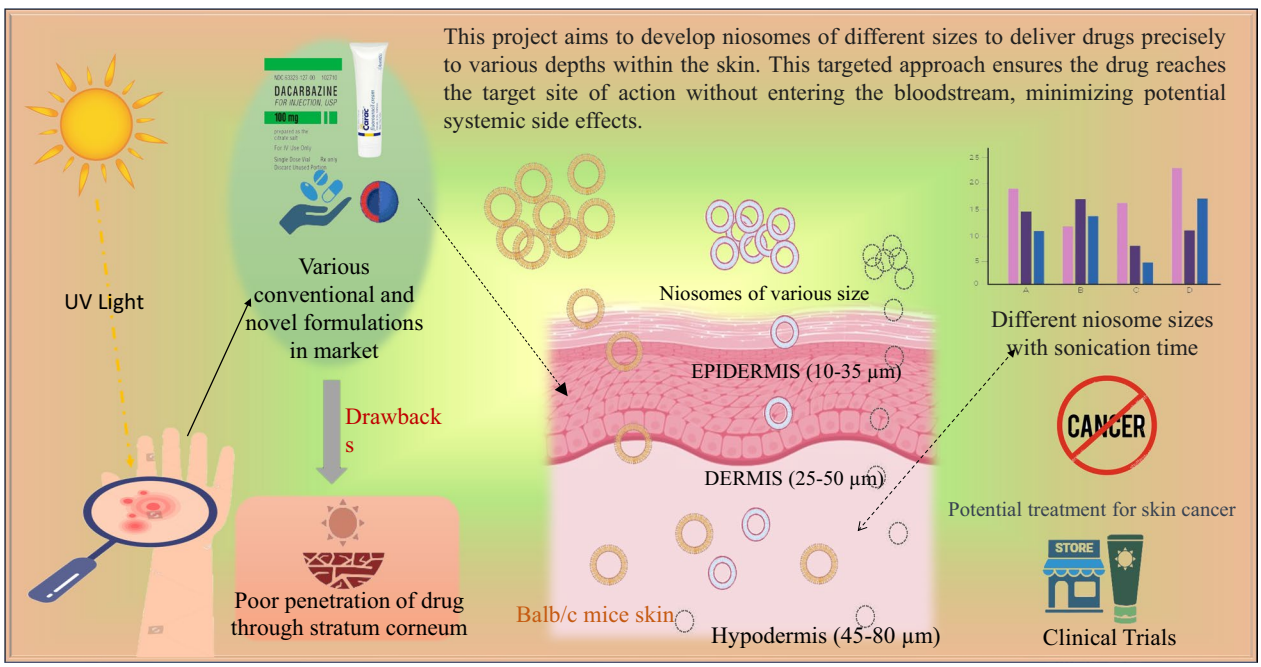

Fig. 2 Schematic representation of niosomes penetration by skin layers

Preparation of MTX-loaded niosomes

The preparation of various niosomal formulations (Nio1 to Nio18) was carried out using the thin-film hydration method but with slight modifications [8, 9], where the mole fraction of Span 60 was systematically varied (4:2:2, 5:2:2, 6:2:2 Soya PC: Cholesterol ratios) while maintaining constant molar concentrations of Soya phosphatidylcholine (SPC) and cholesterol as shown in Fig. 3. An accurate amount of Span 60, soya phosphatidylcholine, and cholesterol was dissolved in a round-bottom flask (RBF) containing 10 mL of chloroform and methanol (9:1). The organic solvents were eliminated using a rotary vacuum evaporator above the lipid transition temperature of 65 °C under reduced pressure to form a thin lipid film on the wall of the RBF. The residual amount of the solvent mixture was removed from the deposited layer of lipids by leaving the contents under a vacuum overnight. Hydration was done with phosphate buffer (PBS 7.4) containing methotrexate drug by rotating the RBF at a suitable temperature for 2 h until the formation of niosomes [22, 23]. The particle size of the formed niosomes dispersion was further reduced by sonication with various sonication cycles. The sonication time is taken as another variable for the formulation process. The same method was used to prepare Rhodamine B-loaded niosomes for the ex vivo study, where 0.5% of the total lipid was substituted with RHB in place of MTX in the selected formulation [10, 24, 25]. The obtained opalescent dispersion of niosomes was stored at 4 ± 2 °C until use.

Characterization of Niosomal formulations

Size distribution, polydispersity, and surface charge of vesicles

Initially, 1 ml of each of the prepared niosomal formulations was mixed with deionized water for adequate dispersion. The average size of the vesicles (VS), the zeta potential (ZP), and the polydispersity index (PDI) of the drug-loaded niosomes was analyzed using Zeta sizer Nano ZS (Malvern Instruments Ltd.) dynamic light-scattering method. The niosomal dispersions were prepared and diluted 10 times with deionized water before measurement to ensure that the light-scattering intensity was within the instrument's detection range [26, 27]. The measurements were taken in triplicate, and the average values are reported in Table 1 and Fig. 4.

Entrapment efficiency (EE)

The entrapment efficiency (EE) was calculated through the mini-column centrifugation method by separating the non-entrapped drug. The %EE of MTX in the niosomes was estimated by determining the free MTX in the dispersion medium. 1 mL of the niosomes dispersion was centrifuged at 15,000 rpm for 2 h at 4 °C using a cooling centrifuge. The supernatant was then separated and diluted, and the concentration of MTX was determined through HPLC methods [11, 28, 29]. The niosomes were then disrupted using 0.1% Triton-X 100, and the drug content is quantified using Eq. (1). An isocratic HPLC procedure was used to determine the concentration of MTX. A Zorbax Extend-C18 column was used as the

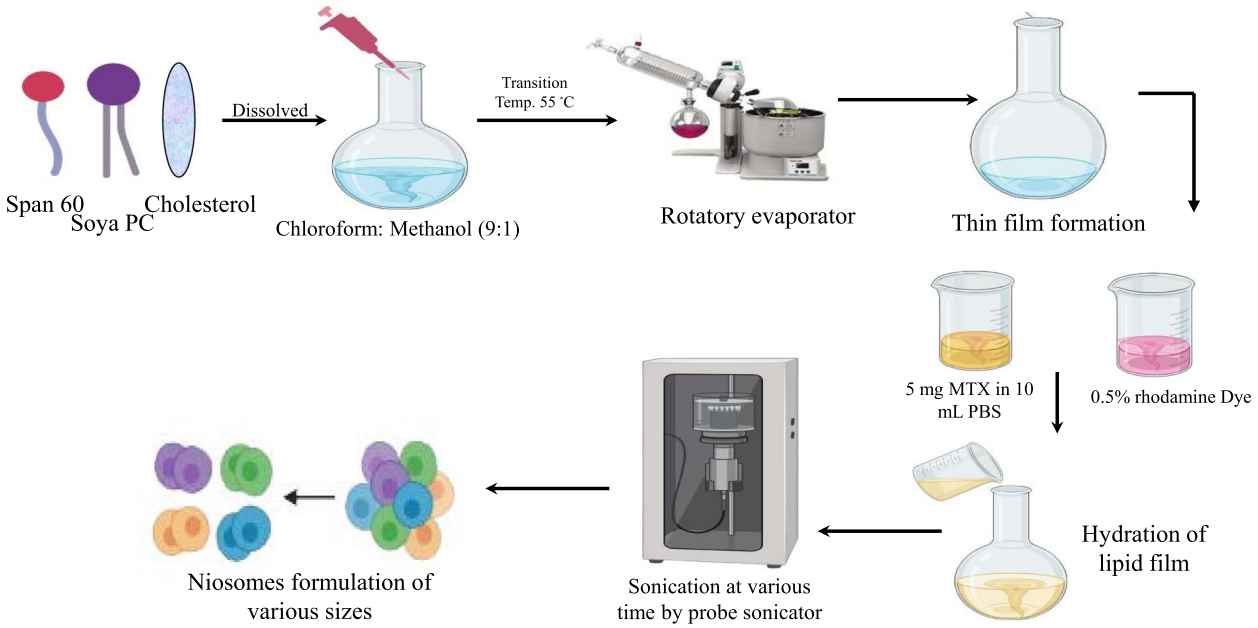

Fig. 3 Method of preparation of niosomes

Table 1 The formulations of niosomes with different ratios of ingredients and sonication time, along with the results of particle sizes, zeta potential, PDI, and entrapment efficiency

Formulation code	Span60:CH:SPC	Sonication time (min)	Vesicle size (nm)	PDI	Zeta potential (mV)	Entrapment efficiency (%)
Nio1	4:2:2	0	1160.3	0.11	− 48.8	68.13
Nio2	4:2:2	2	976.9	0.36	− 45.7	67.43
Nio3	4:2:2	4	843.7	0.44	− 40.3	64.36
Nio4	4:2:2	6	777.5	0.31	− 32.2	58.97
Nio5	4:2:2	8	575.2	0.35	− 38.5	58.04
Nio6	4:2:2	10	289.5	0.43	− 31.2	35.02
Nio7	5:2:2	0	1406.3	0.40	− 54.8	56.23
Nio8	5:2:2	2	965.9	0.23	− 45.7	53.43
Nio9	5:2:2	4	765.7	0.35	− 44.3	48.36
Nio10	5:2:2	6	613.5	0.25	− 40.2	50.97
Nio11	5:2:2	8	535.2	0.33	− 35.5	44.03
Nio12	5:2:2	10	425.5	0.13	− 28.2	30.07
Nio13	6:2:2	0	982.3	0.22	− 38.8	76.23
Nio14	6:2:2	2	783.9	0.30	− 41.7	73.43
Nio15	6:2:2	4	707.7	0.23	− 32.3	56.36
Nio16	6:2:2	6	671.5	0.39	− 27.8	62.97
Nio17	6:2:2	8	597.2	0.49	− 23.3	55.05
Nio18	6:2:2	10	205.2	0.42	− 29.2	50.02

stationary phase, and the mobile phase was a mixture of 50 mM sodium acetate buffer solution with a pH of 5.6 and acetonitrile (89:11 v/v). The flow rate was set at 1.0 mL/min, and the UV detector was set at 307 nm. The results are shown in Table 1 and Fig. 4.

$$\text{Entrapment Efficiency}(\%) = \frac{\text{Amount of free drug}}{\text{Total amount of drug}} \times 100 \quad (1)$$

Shape and surface morphology

The appearance of the optimized MTX-loaded niosomal formulations was studied using the transmission electron microscopy (TEM) technique (Jeol JEM1230, Tokyo, Japan) after suitable dilution. A drop of the selected niosomal dispersion was spread on a copper grid and stained negatively with 1% phosphotungstic acid. The samples were then air-dried for 10 min at standard temperature and pressure (STP) [14, 30, 31] and examined under a TEM as shown in Fig. 5.

Fourier transform infrared spectroscopy

The optimized formulation, drug, excipient, and drug–excipient mixture were analyzed using Fourier transform infrared spectroscopy (FTIR) (Bruker FTIR 8400S ALPHA). Before conducting the IR studies, the samples and excipients were vacuum-dried for 12 h [32, 33]. The dried samples of each were placed on a sample platform, and the spectra were captured in the range of 4000–400 cm^{-1}, which were consistent with the official IR spectrum reported in the monograph as shown in Fig. 6A [12, 13].

Thermoanalytical technique

The thermal characteristics of pure methotrexate (MTX), Soya Phosphatidylcholine (PC), Cholesterol, Span 60, the physical mixture of MTX and niosomal components, empty niosomes, and MTX-loaded niosomes were analyzed using differential scanning calorimetry technique (DSC 60, Shimadzu, Japan). The device was calibrated using high-purity indium (99.9%). Three milligrams of accurately weighed samples were put into standard aluminum pans and then heated from 100 to 300 °C at a scanning rate of 100 °C per minute [15, 34, 35] as shown in Fig. 6B.

In vitro drug release kinetics

The niosomal suspension (Nio 15 and Nio 16) was centrifuged to separate the unentrapped drug from the niosomes. Next, 1 mL of the pure niosomal suspension was placed into a dialysis tube, which was then immersed in a beaker that contained 20 mL of PBS (pH 7.4) and stirred on a magnetic stirrer at a constant temperature of 37 ± 0.5 °C. Samples were taken at various time intervals

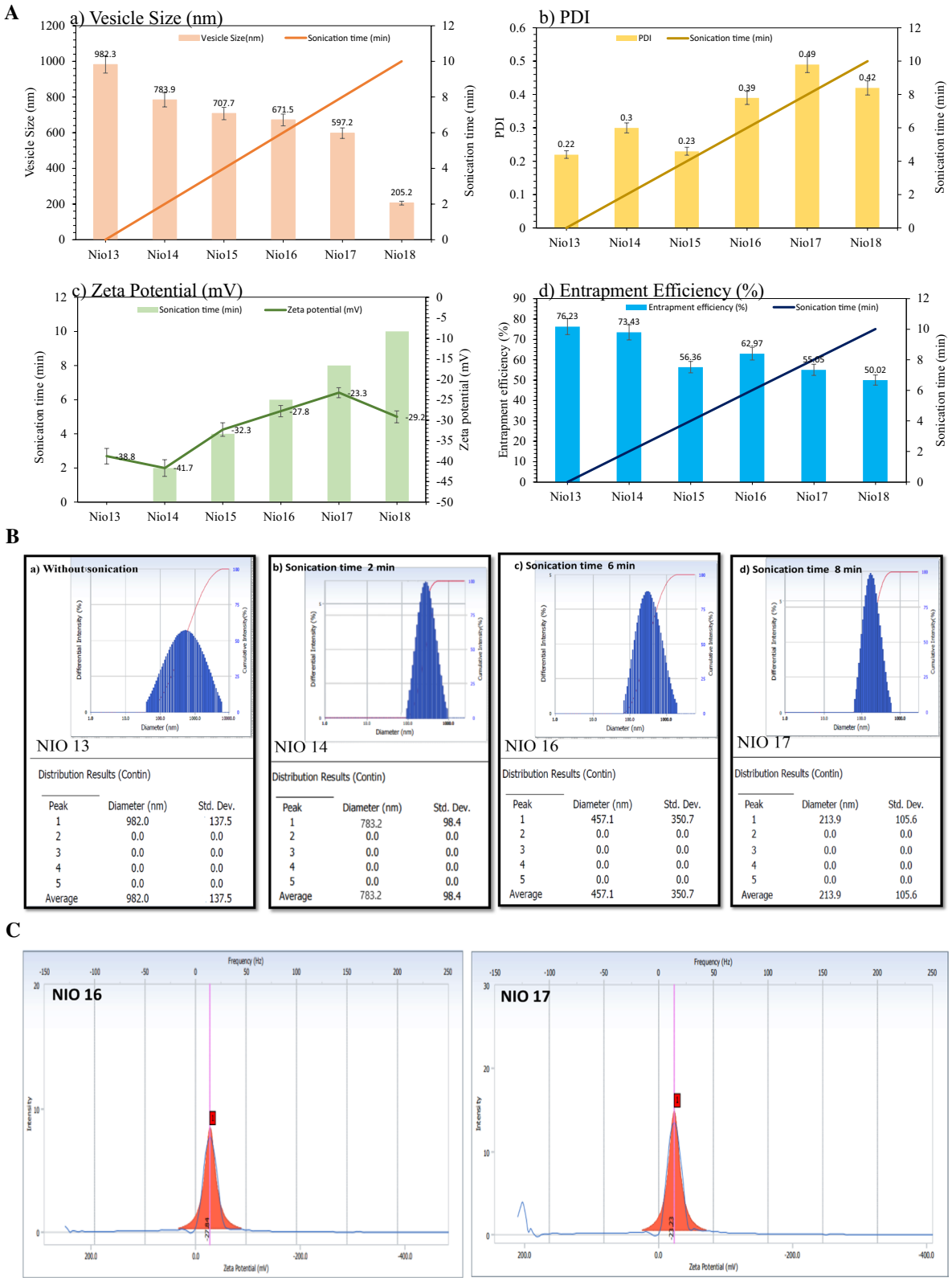

Fig. 4 **A** Graphical representation of formulation optimization with ratio 6:2:2 (Span 60:CH:SPC); **a** vesicle size (nm); **b** PDI; **c** Zeta Potential (mV); **d** entrapment efficiency (%). **B** Images showing the particle-size distribution of the optimized formulations (NIO 13, 14, 17, and 18) prepared using a ratio of Span 60:CH:SPC (6:2:2). **C** Images showing the zeta potential of the optimized formulations (NIO 16 and 17) prepared using a ratio of Span 60:CH:SPC (6:2:2)

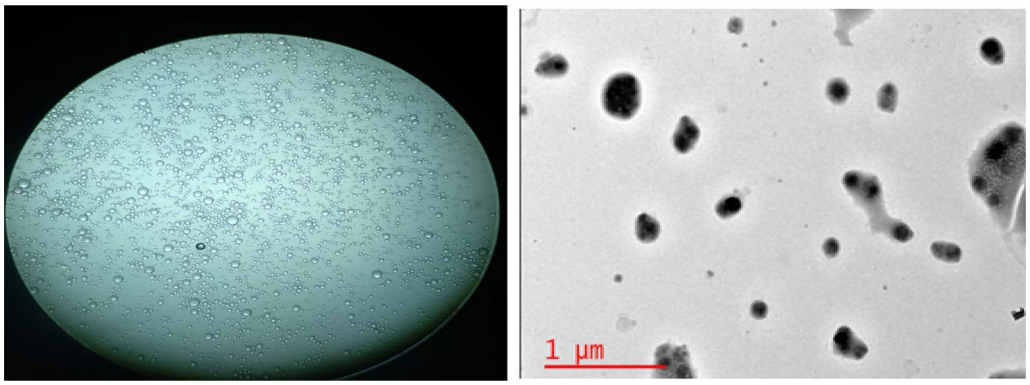

Fig. 5 Fluorescent and TEM images of niosomes

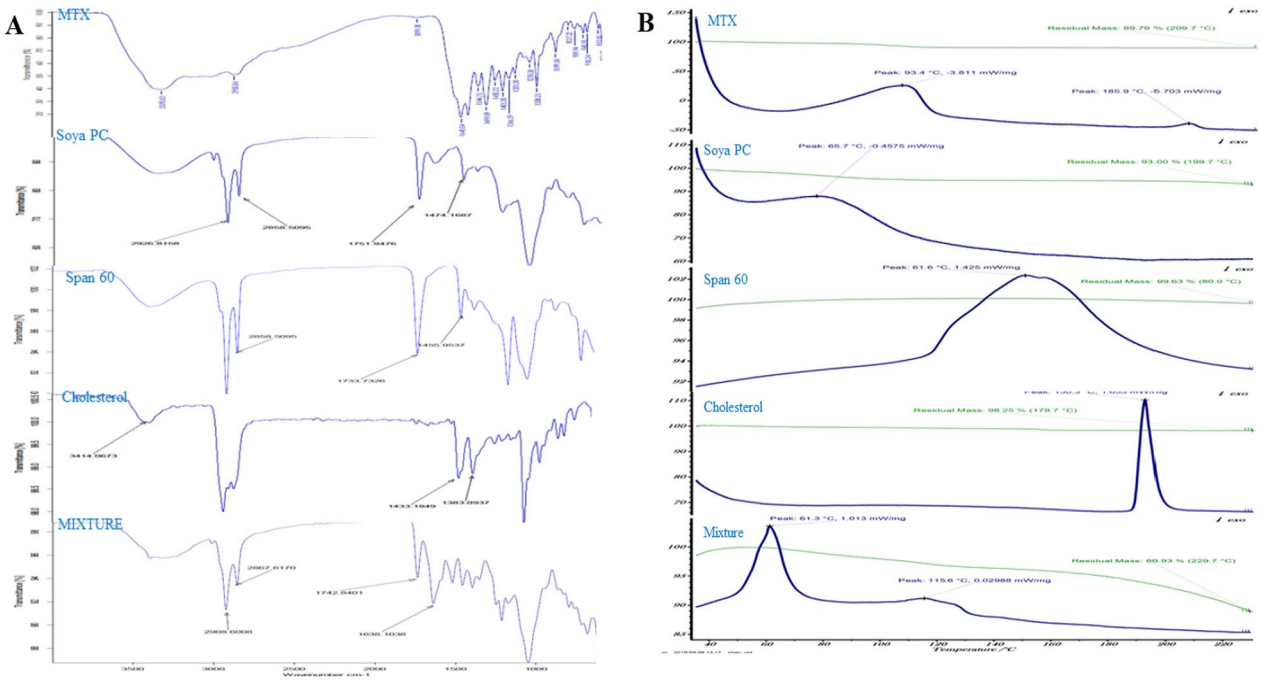

Fig. 6 **A** FTIR spectra of methotrexate, Soya PC, Span 60, Cholesterol and Mixture; **B** DSC spectra of methotrexate, Soya PC, Span 60, cholesterol and mixture

and analyzed for drug content using HPLC. To maintain the initial volume of the dissolution fluid, 5 mL of fresh solution was added after each sample withdrawal [15, 20, 36, 37]. The cumulative amount of MTX released from different niosomal formulations was calculated as per Eq. (2). Results are shown in Fig. 7.

$$\text{Percentage cumulative drug released} = \frac{\text{Cumulative Amount of Drug obtained at time}}{\text{Total amount of Drug in Niosomes}} \quad (2)$$

In vitro cytotoxicity study

In vitro, cell cytotoxicity of optimized formulation (Plain MTX, NIO 5, NIO 12, and NIO 16) was evaluated by the SRB assay using murine skin melanoma cell line B16-F10. The cell lines were grown in RPMI 1640 medium, and cells were inoculated into 96-well plates in 100 µL

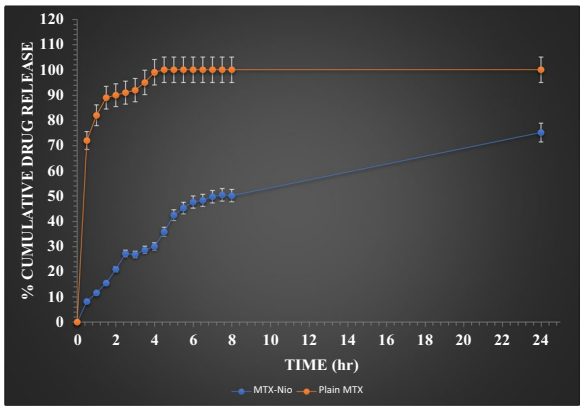

Fig. 7 In vitro release of MTX from niosomes in comparison to plain MTX solution at pH 7.4

at plating [38–40]. After cell inoculation, the microtiter plates were placed in an incubator at 37 °C, 5% CO_2, 95% air, and 100% relative humidity for 24 h before the addition of formulations. Formulations were dissolved in an appropriate solvent to a concentration of 100 µg/mL and then diluted to 1 mg/mL using Milli-Q water. The diluted solutions were stored frozen until needed. At the time of the experiment, aliquots of the frozen concentrate (1 mg/mL) were thawed and diluted to the following concentrations: 100 µg/mL, 200 µg/mL, 400 µg/mL, and 800 µg/mL. Aliquots of 10 µL of each drug dilution were added to microtiter wells that already contained 90 µL of the medium. This resulted in final drug concentrations of 10 µg/mL, 20 µg/mL, 40 µg/mL, and 80 µg/mL. The plates were then incubated at standard conditions for 48 h.

To terminate the assay, cold TCA was added to the plates. Cells were fixed in situ by gently adding 50 µL of cold 30% (w/v) TCA (final concentration, 10% TCA) [41, 42]. The plates were then incubated for 60 min at 4 °C. The samples were washed five times with PBS, and then, 50 µL of 0.4% (w/v) SRB solution was added to each well. The plates were then incubated for 20 min at room temperature.

One percent (v/v) of acetic acid was used to remove the unbound dye, and plates were dried and then analyzed at the wavelength of 540 nm with a 690 nm reference wavelength by using the plate reader. Adriamycin (ADR) was used in the same concentration range as a positive control. Cytotoxicity was expressed as the percentage of viable cells relative to incubated cells in the presence of 0.1% DMSO vehicle control. The percentage of growth inhibition (GI_{50}) is calculated in Eq. (3). GI_{50} was calculated from the drug concentration, resulting in a 50% reduction in cell growth. Each measurement was done in triplicate [18, 19, 43]. Results shown in Fig. 8.

$$\text{Percentage growth inhibition} = (\text{Ti} - \text{Tz})/(C - \text{Tz}) \times 100 \quad (3)$$

where absorbance at zero time (Tz), control growth (C), and test growth of formulation in the presence of drug at four concentration levels (Ti).

Ex vivo and in vivo investigations

The ex vivo investigation was conducted following protocols approved by the Committee for Control and Supervision of Experiments on Animals (CPCSEA/SN-10/RN-22/16-02-2020), which is overseen by the Ministry of Social Justice and Empowerment, Government of India. The study also followed the recommendations of the Institutional Animal Ethical Committee (IAEC) at Dr. H.S. Gour Vishwavidyalaya, located in Sagar, Madhya Pradesh, India.

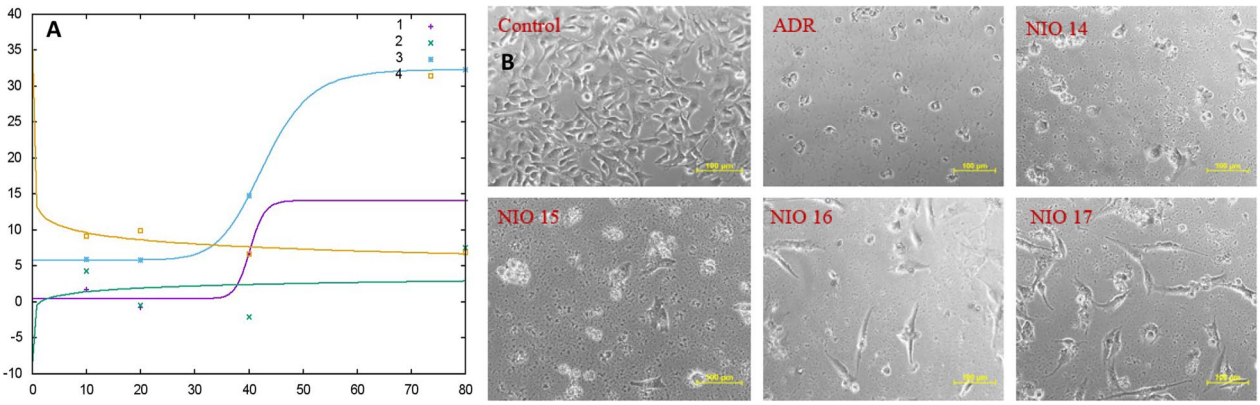

Fig. 8 **A** Growth curve: the plot of percentage growth inhibition versus drug concentration (µg/mL) shows the effective drug concentration on murine tumor cell line B16 F10 cells; **B** Phase-contrast microscopic images of murine tumor cell line B16 F10 cells after 24 h. treatment negative control (untreated), ADR, and formulations NIO 14 to NIO 17

Ex vivo permeation study

The ex vivo visualization using confocal laser scanning microscopy technique (CLSM) involved the formulation of Rhodamine B (RH)-loaded niosomes through a process similar to that used for creating MTX-loaded niosomes [44–46]. However, RH was incorporated at a concentration of 0.5% concerning the total lipid content, replacing MTX in the specific formulation. For experimentation, the mice's skin was sectioned into square pieces and positioned with the stratum corneum (SC) facing the donor compartment within diffusion cells. The receptor chamber contained 20 mL of phosphate buffer saline (pH 7.4) maintained at 32 ± 1 °C. To mimic the expected application of niosomes to the skin's surface, RH-loaded niosomes (including a plain niosomes formulation, a plain rhodamine solution, and formulations Nio 13 to Nio 17) were administered onto the skin and allowed to remain for 4 h. Following this, the skin was rinsed with 10% ethanol and then gently wiped in preparation for imaging, following the methods described by [16, 47]. The investigation of the skin was conducted using CLSM with the following steps: the complete skin sample was positioned between a glass slide and a cover slip and examined utilizing inverted CLSM (LSM 710, Carl Zeiss, Jena, Germany). RH fluorescence was excited at a wavelength of 573 nm and detected at 591 nm. Scans were taken at 2-µm intervals starting from the skin surface (0 mm) to a depth of 40 µm, using a 40× objective lens. Images shown in Fig. 9 were captured in both the *xy* and *xz* planes, employing optical sectioning z-stack mode. The acquired confocal microscopy images were processed using LSM Image Browser software, release 4.2 (LASX), as described by Hathout and Nasr in 2013 [17, 48].

In vivo histopathological study

An In vivo histopathological study was performed to evaluate skin irritation potential and structural changes resulting from exposure to MTX-loaded niosomes. The study involved dividing mice into 7 groups, each consisting of 3 animals [49, 50]. Group I acted as the positive control receiving PBS, group II as the negative control receiving plain MTX solution, and groups III to VII were exposed to topical applications of MTX-encapsulated niosomes (Nio 13 to 17) on the skin surface three times daily for a week. After the treatment period, the mice were killed, and their skin was extracted for histopathological examination. The collected skin samples underwent fixation in 10% formal saline for 24 h, followed by washing, dehydration using alcohol dilutions, clearing in xylene, and embedding in paraffin beeswax blocks. These blocks were maintained at 56°C for 24 h, and sections of 4 mm thickness were cut using a microtome (Leica Microsystems SM2400, Cambridge, England). These sections were then deparaffinized, stained with hematoxylin counterstained with eosin, and subsequently observed under a light microscope for analysis as shown in Fig. 10 [9, 21, 51].

Results and discussion

Preparation of niosomal formulation, particle-size analysis, and zeta potential determination

The synthesis of MTX-loaded niosomes was achieved using the film hydration method as depicted in Fig. 3 and by incorporating various ratios of span 60, soya PC, and cholesterol in each formulation. The study aimed to determine the effect of various ingredients and processing variables on the vesicle size and entrapment efficiency. The composition of span 60, soya PC, and cholesterol (4:2:2, 5:2:2, 6:2:2) had a significant impact on the size of the niosomes. The results showed that increasing

(See figure on next page.)

Fig. 9 **A** Confocal laser scanning photomicrographs illustrating a *z*-stack image capturing optical sections of mice skin. The sections were taken at intervals of 2 µm, covering a depth range from 0 to 38 µm. The formulations employing PBS as a positive control exhibit no observable particles. **B** Confocal laser scanning photomicrographs illustrating a *z*-stack image capturing optical sections of mice skin. The sections were taken at intervals of 2 µm, covering a depth range from 0 to 38 µm. The formulations employing Plain Rhodamine as a negative control exhibit no observable particles. **C** Confocal laser scanning photomicrographs illustrating a *z*-stack image capturing optical sections of mice skin. The sections were taken at intervals of 2 µm, covering a depth range from 0 to 14 µm. The formulations using Nio13 (Without Sonication) as an agent demonstrate the presence of particles, visible within the range of 0–6 µm. **D** Confocal laser scanning photomicrographs illustrating a *z*-stack image capturing optical sections of mice skin. The sections were taken at intervals of 2 µm, covering a depth range from 0 to 14 µm. The formulations using Nio14 (2 min Sonication) as an agent demonstrate the presence of particles, visible within the range of 4–18 µm. **E** Confocal laser scanning photomicrographs illustrating a *z*-stack image capturing optical sections of mice skin. The sections were taken at intervals of 2 µm, covering a depth range from 0 to 14 µm. The formulations using Nio15 (4 min Sonication) as an agent demonstrate the presence of particles, visible within the range of 16–22 µm. **F** Confocal laser scanning photomicrographs illustrating a z-stack image capturing optical sections of mice skin. The sections were taken at intervals of 2 µm, covering a depth range from 0 to 40 µm. The formulations using Nio16 (6 min Sonication) as an agent demonstrate the presence of particles, visible within the range of 24–32 µm. **G** Confocal laser scanning photomicrographs illustrating a *z*-stack image capturing optical sections of mice skin. The sections were taken at intervals of 2 µm, covering a depth range from 0 to 38 µm. The formulations using Nio17 (8 min Sonication) as an agent demonstrate the presence of particles, visible within the range of 12–38 µm

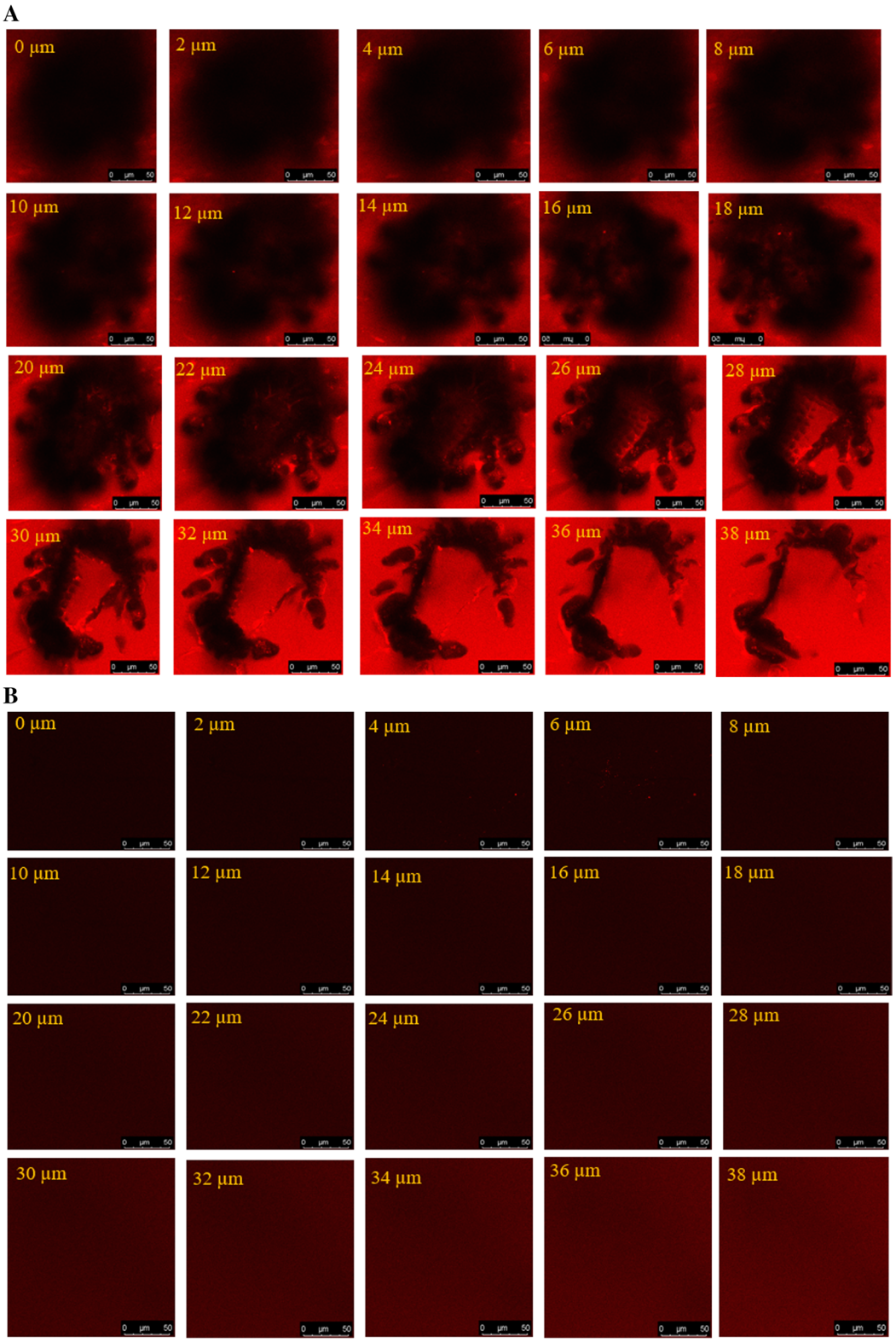

Fig. 9 (See legend on previous page.)

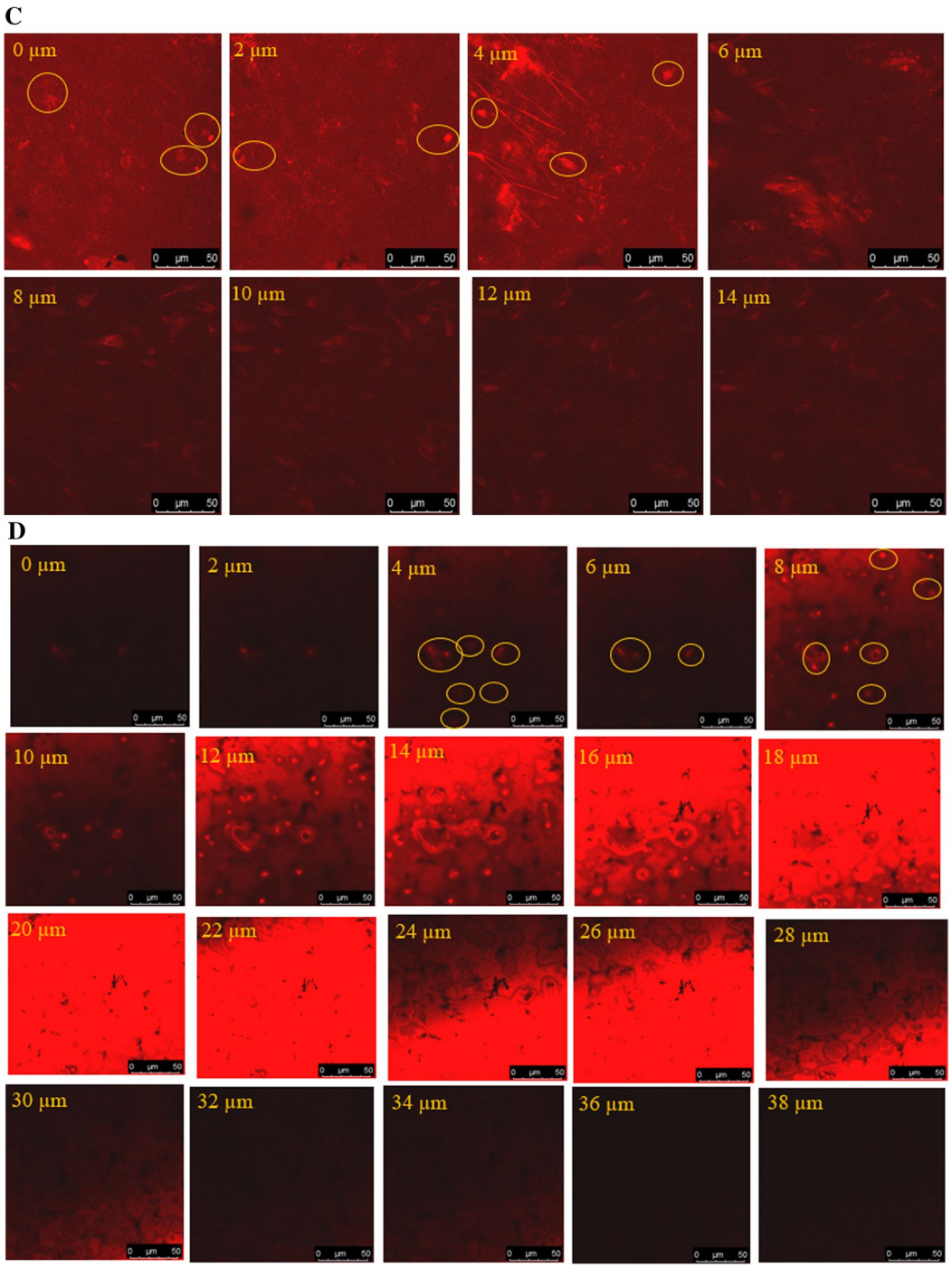

Fig. 9 continued

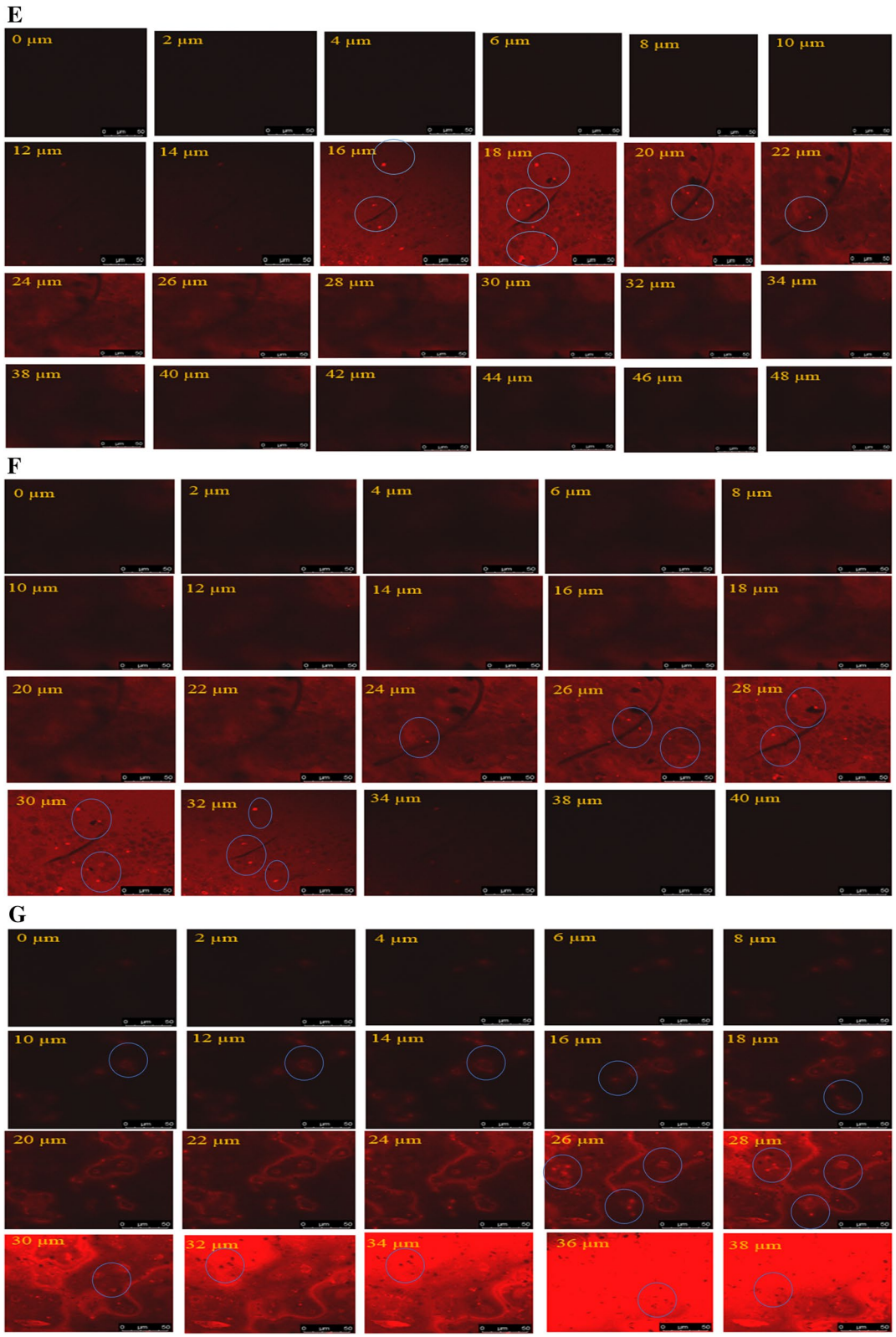

Fig. 9 continued

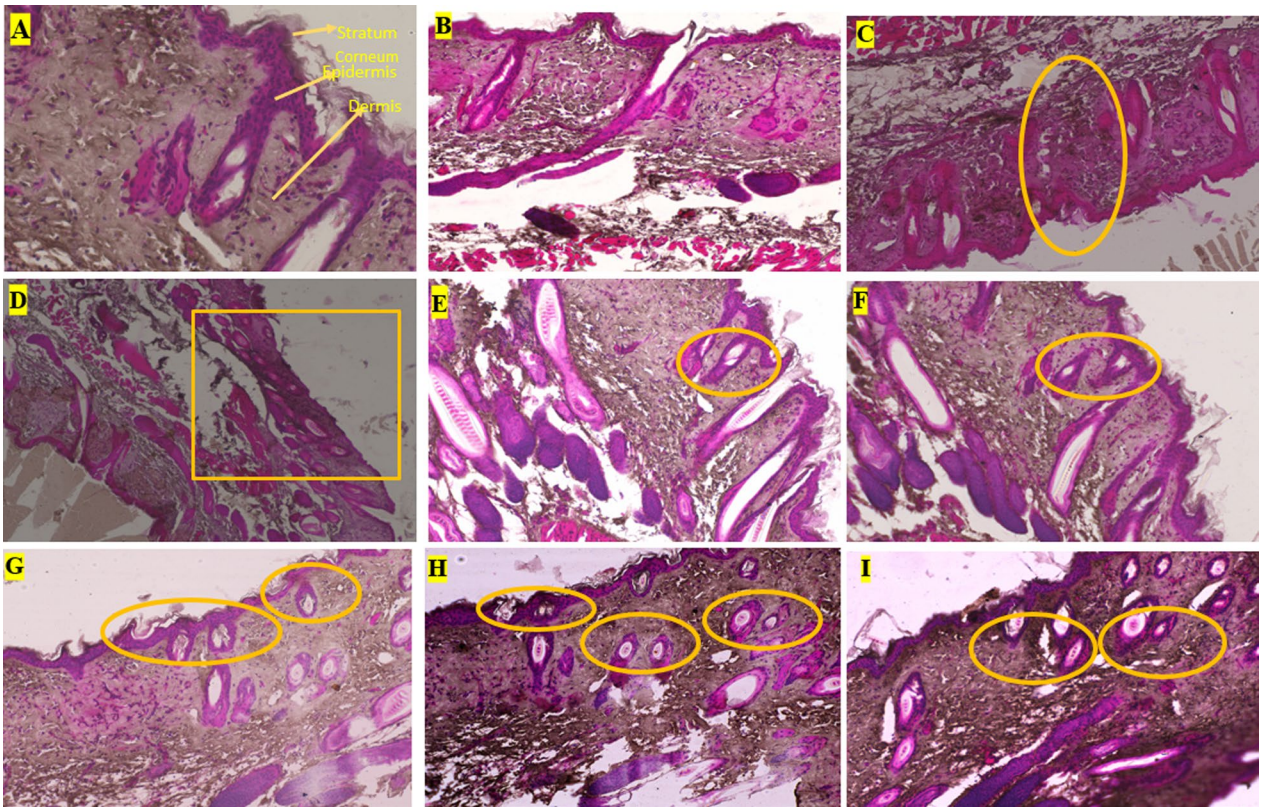

Fig. 10 Photomicrographs showing histopathological sections (hematoxylin and eosin stained) of mice skin **A** normal untreated, **B** treated with Plain MTX, **C** Nio13, **D** Nio14 **E**, **F** Nio15, **G**, **H** Nio16 and I: Nio17. The magnification power of 40× to identify the epidermis, dermis, the subcutaneous tissue and muscles, respectively

the concentration of Span 60 (a non-ionic surfactant with an HLB of 4.7) led to a decrease in vesicle size. This is because Span 60 has high interfacial activity and a critical packing parameter (CPP) between 0.5 and 1. A lower CPP indicates that the surfactant molecules are more tightly packed, which results in smaller vesicles. However, a further increase in the concentration of Span 60 led to an increase in vesicle size. This is because the higher concentration of cholesterol in the vesicles provided added rigidity, which counteracted the effect of the increased interfacial activity of Span 60. The addition of cholesterol in lipid vesicles changes the short-distance repulsive forces among them. An increase in cholesterol content leads to an increase in the net repulsive forces among soya PC and span 60 vesicles, reducing their aggregation. The sonication time also affects the entrapment efficiency and size of MTX-loaded niosomes, as seen in Table 1. An increase in sonication time causes a decrease in particle size. Particles without sonication showed the largest size, while particles subjected to 10 min of sonication showed the smallest size, with a mean particle size ranging from 200 to 1406 nm. The optimized formulations, with a ratio of 6:2:2, were used for further studies. The average standard deviation (SD) (nm) of particle size for most of the particles was 200–1000 nm, depending on the sonication time cycle, and the polydispersity index was less than 0.4. The formulations had a negative zeta potential of −25 to −30 mV as depicted in Fig. 4A, B and showed the best entrapment efficiency. The negative zeta potential of the formulations assisted in their adhesion to cancer cells and internalization through cellular endocytosis.

Entrapment efficiency

After removing the unencapsulated drug through dialysis, the efficiency of encapsulation was analyzed for all the formulations. The presence of surfactant, cholesterol, and drug-to-lipid ratios in the vesicles can reduce the stiffness of the vesicles and affect the ability of methotrexate to be trapped inside. The highest drug encapsulation efficiency was recorded to be 76% in vesicles without sonication and the lowest was 30% with a 10-min sonication cycle.

Shape and surface morphology

Confirmation of the results obtained from the Malvern particle-size analyzer can be achieved through

morphological analysis, which also examines the structure of colloidal systems. The optimized niosomes displayed a non-aggregated, single-layered vesicular structure with a predominant spherical shape as seen in the TEM images (Fig. 5). The average particle size observed in the TEM micrographs was consistent with the size previously obtained from the Malvern particle-size analyzer, as presented in Table 1.

Fourier transform infrared spectroscopy (FTIR)

FTIR spectroscopy is a useful tool in determining potential interactions between drugs and excipients. Figure 6A shows the IR spectra of pure methotrexate and a formulation that includes the drug and other excipients like phospholipids and a permeation enhancer. The pure methotrexate exhibits peaks at 3406.10 cm^{-1} (N–H stretching), 2928.64 cm^{-1} (O–H stretching for the carboxylic group), 1646.82 cm^{-1} (C–C stretching), 1603.41 cm^{-1} (C=C stretching of aromatics), 1542.02 cm^{-1} (N–H bend), and 831.01 cm^{-1} (C–H out of the plane of aromatics). The peaks for span 60 were found at 2950.00, 2856.50, and 1733.73 cm^{-1}, while peaks for lipids were observed at 3414.06, 2875.67, 1383.09, 1433.18, 1056.43, and 1547.14 cm^{-1}. Peaks for phosphatidylcholine (PC) were recorded at 3467.98, 2926.81, 1474.01, 1214.58, and 1042.76 cm^{-1}. The prepared formulations were also analyzed and found to have peaks in the same range, the drug and the lipid did not interact. The peaks of the optimal formulation were found to be very similar to those of the pure methotrexate, i.e., 3500.00, 3100.00, 2908.60, 1742.64, 1638.10, 1510.00, 1540.21, 1210.12, and 815.00 cm^{-1}, revealing that there was no significant change in the IR peaks of methotrexate and the optimized formulation, signifying the compatibility of the drug and the polymer.

Thermoanalytical technique

Figure 6B displays the DSC (differential scanning calorimetry) thermograms of various substances, including pure methotrexate (MTX), Soya phosphatidylcholine (PC), cholesterol, Span 60, a physical mixture of MTX with niosome components, blank niosomes, and MTX-loaded niosomes. The thermogram of MTX exhibits a typical exothermic peak at 185.9 °C and 93.5 °C, indicating its crystalline form, with a residual mass of 89.79% and weight loss of 7.79%. The thermogram of Span 60 displays a characteristic endothermic peak resulting from melting at 61.6 °C, with a residual mass of 93.00% and weight loss of 3.82%. The thermogram of cholesterol indicates an endothermic peak due to melting at 121.6 °C and 150.3 °C, with a residual mass of 98.25% and weight loss of 2.75%. The DSC of the physical mixture of MTX with niosome components reveals the peaks of both Span 60 and Soya PC, as well as the MTX peak, indicating that it maintains its crystalline form. However, the decrease in MTX peak intensity may be related to the dilution effect caused by the excipients. The thermogram of the unloaded niosomes demonstrates the absence of the MTX characteristic peak. The endothermic peak of Span 60 is present in both the blank niosomes and drug-loaded niosomes but shifted to a lower temperature (61.6 °C). For the drug-loaded niosomes, the MTX characteristic peak is completely gone, which could indicate that MTX was either encapsulated inside the niosomes or transformed into a molecular state within the surfactant mixture. As reported by Nasr et al. (2013) [17], the absence of the drug's crystalline melting peak after encapsulation may also indicate the presence of a strong interaction between the surfactant bilayers of the vesicles and the entrapped drug.

In vitro drug release kinetics

Figure 7 depicts the in vitro release profile of the optimized niosomal suspension loaded with methotrexate at pH 7.4 and 35 ± 0.5 °C. The optimized formulation exhibited a cumulative drug release of 75.09% over 24 h. The release curve indicated an initial burst release where approximately 28% of the drug was released within the first two and a half hours. The subsequent drug release from the optimized niosomes was sustained. The initial burst release was attributed to the presence of free methotrexate in the external phase.

In vitro cell proliferation studies

The anti-cancer efficacy of the formulations Plain MTX, NIO 5, NIO 12, and NIO 16 was tested against the murine skin melanoma cell line B16-F10 using the SRB assay, with ADR (Adriamycin) serving as a positive control. Figure 8A, B shows the activity of the formulations against B16-F10 cells. The results, presented in Table 2, indicate that NIO 16 was significantly more effective than other formulations like NIO 5 and Nio12. The GI_{50}

Table 2 Cytotoxic effects of formulations NIO 14 to NIO 17 on murine tumor cell line B16F10 cells

Treatment	% Growth inhibition at concentration (µg/mL)				GI_{50} (µg/mL)
	10	20	40	80	
NIO 14	9.1	9.9	6.7	6.9	2.5311
NIO 15	4.3	− 0.5	− 2.1	7.5	8.05738
NIO 16	1.7	− 0.8	6.7	14.1	40.2238
NIO 17	5.9	5.8	14.8	32.3	38.7176
ADR	− 70.5	− 72.1	− 73.4	− 56.4	2.16266

values were 8.05738 µg/mL (NIO 5), 2.5311 µg/mL (NIO 12), 38.7176 µg/mL (NIO 16), and 40.2238 µg/mL (Plain MTX). The investigation revealed that Nio16 (with a GI50 of 38.7176 µg/mL) exhibited considerable potential in countering cancer activity within B16-F10 cells. It displayed enhanced efficacy in curbing cell growth when contrasted with alternative formulations. This heightened effectiveness might be attributed to potential factors such as the diffusion of niosomes from the stratum corneum, the amplification of permeation through the influence of Span 60 surfactants present in the niosomal formulation, or even modifications to the stratum corneum to augment the permeability of the intercellular lipid barrier. The drugs (MTX) can cross through the niosomes due to their interactions with aggregation, fusion, and adhesion, leading to a large thermodynamic gradient. Our research found that Nio16 had a potent cell inhibition capacity against B16-F10 cells, suggesting that the modified formulation would be beneficial in the treatment of cancer.

Ex vivo and In vivo investigations

Ex vivo skin penetration study

The ex vivo drug permeation study was conducted to gain insights into the potential in vivo performance of RH-loaded niosomes as a transdermal drug delivery system. Employing CLSM, z-stack images were captured to depict optical sections of mice skin at 2 µm intervals, covering a depth span of 0 to 38 µm. Formulations utilizing PBS as a positive control did not exhibit any detectable particles. Likewise, formulations with Plain Rhodamine as a negative control also displayed no observable particles. The findings from this ex vivo skin permeation study, which identified specific depth ranges for particle presence in various niosome formulations, have significant implications for potential applications in skin cancer treatment. Notably, Nio13 (982.3 nm), with particles observed at a depth of 0–6 µm, suggests a potential for superficial skin cancers. Nio14 (783.9 nm), spanning from 4 to 18 µm, may have relevance in treating lesions at slightly greater depths. The formulation Nio15 (707.7 nm), demonstrating distinct particles between 16 snf 22 µm, could be well-suited for targeting tumors residing slightly deeper within the skin. For more deeply seated skin cancers, Nio16 (671.5 nm), with particles at depths ranging from 24 to 32 µm, may offer a solution. Additionally, Nio17 (597.2 nm), with particles distributed within a broad range of 12 to 38 µm, could be instrumental in addressing skin cancers with varying depths or infiltrative characteristics. The particles of Nio 18 (205.0 nm) will go into systemic circulation. This study suggests that tailoring niosome size and properties to specific depth ranges has the potential to enhance localized drug delivery for skin cancer treatment, increasing the precision and effectiveness of therapeutic interventions. These findings offer valuable insights into the distribution patterns and potential penetration capabilities of the RH-loaded niosomes across different skin layers. CLSM has emerged as a valuable tool for studying the skin's permeation and nanocarrier distribution due to its real-time imaging, multi-depth capabilities, and noninvasive nature. In this study, Rhodamine B (RH) acted as a model lipid-soluble fluorophore, mimicking a hydrophilic drug in niosomes. Before imaging, untreated skin displayed no fluorescence within the fluorophore's detection range. The visualizations (Fig. 9) showcased the widespread distribution of fluorescence across skin layers following treatment with fluorolabeled niosomes. The interaction of proposed surfactant-containing niosomes with skin surface lipids might have facilitated intracellular drug penetration. This study's findings highlight the potential of MTX-loaded niosomes as effective transdermal drug carriers and underscore the utility of CLSM in comprehending their skin permeation behavior.

In vivo histopathological study

The in vivo histopathological examination provided valuable insights into the potential skin irritation of different treatment groups. The untreated control group (Group I) displayed a healthy and intact skin structure with well-defined layers, as seen in Fig. 10. This serves as a baseline for comparison. Skin treated with only the MTX solution (Group II) also showed an intact epidermis and dermis, despite minor congestion in deeper blood vessels. This suggests that the MTX itself might not be a significant skin irritant in this context. Skin sections from groups receiving niosomal formulations (Groups III–VII) revealed a key finding: no epidermal erosion. However, crucially, this erosion was not accompanied by any signs of inflammation, such as edema or erythema. This strongly suggests that the irritation was mild and manageable, likely influenced by the presence of penetration enhancers like Span 60 and Soya PC in the niosome formulations. Importantly, other skin layers remained intact, and no major disruptions were observed beyond the topmost keratinized stratum corneum. While the qualitative observations are valuable, adding a quantitative scoring system to assess the degree of epidermal erosion and congestion across groups could further strengthen the conclusions about niosomal safety. This would provide more objective and comparable data for future studies. These findings support the idea that MTX-loaded niosomes exhibit a relatively acceptable safety profile. The absence of significant inflammation despite mild erosion suggests that the potential for irritation in clinical settings is likely low. However, future studies implementing quantitative scoring would further bolster these conclusions and

provide even more robust evidence for the safety of these niosomes as drug delivery systems.

Discussion

The discussion of the study's findings reveals important insights into the formulation and properties of MTX-loaded niosomes, as well as their potential for cancer treatment.

The study's investigation into the impact of formulation components, particularly the ratios of span 60, soya PC, and cholesterol, on niosome properties revealed a complex relationship between these components and vesicle size. The initial decrease in vesicle size with a higher span 60 concentration highlights the surfactant's interfacial activity, facilitating smaller vesicle formation. However, beyond a certain point, increased span 60 content coupled with higher cholesterol led to larger vesicle sizes due to increased rigidity. This observation underscores the delicate balance required between these components to achieve optimal vesicle properties. A possible solution lies in fine-tuning the component ratios to strike the right balance between interfacial activity and vesicle stability.

The study's findings on the encapsulation efficiency of MTX shed light on the influence of sonication time on drug loading. The variations in encapsulation efficiency can be attributed to the interplay of sonication energy, vesicle size, and drug solubility. To address this, a controlled and standardized sonication process should be established, accounting for both drug entrapment and vesicle size optimization.

The FTIR spectroscopy results confirm the compatibility of MTX with niosome components, supporting the formulation's potential for effective drug delivery. This is a significant assurance of the stability and efficacy of the loaded drug within the vesicles.

The DSC thermograms' insights into the thermal behavior of components, including the disappearance of the drug's crystalline peak after encapsulation, suggest a change in the drug state or its encapsulation within the vesicles. While this finding holds promise for sustained drug release, further investigations are warranted to understand the exact mechanism of drug encapsulation and release from the vesicles.

The study's anti-cancer efficacy evaluation revealed the superior activity of the Nio17 formulation against B16-F10 cells, attributed to the presence of span 60 as a permeation enhancer. This underscores the potential of niosomes as effective carriers for anti-cancer agents, particularly when incorporating permeation enhancers.

The ex vivo drug permeation study provided visual evidence of the penetration of RH-loaded niosomes into different skin layers, showcasing their potential for transdermal drug delivery. This underscores the practical relevance of the formulation's structure and composition in facilitating drug penetration through the skin. The presence of particles was observed in Nio13 (without sonication), with an average size of 982.3 nm (nm) visible within 0 to 6 μm (μm). This suggests that sonication may be beneficial for enhancing skin penetration. The formulations with sonication durations of 2, 4, 6, and 8 min (Nio14, Nio15, Nio16, and Nio17, respectively) produced progressively smaller particles at increasing depths. The particle sizes ranged from 783.9 nm (4–18 μm), 707.7 nm (16–22 μm), 671.5 nm (24–32 μm), to 597.2 nm (12–38 μm), indicating improved permeation. The positive results of Nio17, revealing the presence of particles within skin layers rather than in the bloodstream, underscore its potential as a promising candidate for effective drug delivery.

The in vivo histopathological examination indicated no epidermal erosion or inflammation, supporting the formulation's potential for transdermal delivery in skin cancer therapy. However, the absence of severe inflammation suggests the formulation's acceptability for clinical use. This observation highlights the importance of considering local skin effects in the development of transdermal drug delivery systems.

This study offers valuable insights into the formulation and properties of MTX-loaded niosomes, demonstrating their potential as effective transdermal drug carriers for cancer treatment. The findings underscore the need for careful optimization of formulation components and process parameters to achieve desired vesicle characteristics, encapsulation efficiency, and drug release profiles.

Conclusion

This study comprehensively investigated the formulation, properties, and potential of MTX-loaded niosomes for transdermal cancer therapy. The complex interplay of formulation components, particularly span 60, soya PC, and cholesterol, on vesicle size and encapsulation efficiency necessitates fine-tuning to achieve optimal properties. Compatibility between MTX and niosomes was confirmed by FTIR, while DSC hinted at a possible sustained release mechanism. Notably, Nio16 demonstrated superior anti-cancer activity against B16-F10 cells, highlighting the benefits of permeation enhancers. Ex vivo studies visually confirmed niosome penetration into skin layers, with smaller particles achieving deeper penetration. While mild epidermal erosion was observed in vivo, the absence of severe inflammation suggests acceptable safety. This study establishes the promising potential of MTX-loaded niosomes for transdermal cancer treatment, emphasizing the importance of optimizing formulation parameters and exploring complementary techniques

like CLSM for further validation. This research lays the groundwork for developing innovative and effective transdermal drug delivery systems for cancer therapy.

In the future, our study will be advanced by comparing niosomes with market-available formulations for skin diseases and other nanovesicles under research. Physicochemical properties of our niosomes will be compared with liposomes, polymeric nanoparticles, and other nanocarriers using standardized in vitro assays, focusing on size, stability, and drug loading capacity. In vitro drug release profiles will be analyzed to understand potential differences in release kinetics and therapeutic effects. Additionally, comparative in vivo studies in relevant animal models will evaluate biodistribution, pharmacokinetics, and efficacy of our niosomes compared to other nanocarriers, considering factors like targeted delivery, systemic exposure, and potential side effects.

Abbreviations

MTX	Methotrexate
PC	Phosphatidylcholine
TEM	Transmission electron microscopy
FTIR	Fourier transform infrared spectroscopy
DSC	Differential scanning calorimetry
GI50	Growth inhibition concentration at 50%
CLSM	Confocal laser scanning microscopy

Acknowledgements
Authors acknowledge AICTE GPAT Fellowship for providing funding opportunity and thank the Sophisticated Instrument Center of Dr. Harisingh Gour University, Sagar, India, for providing the instrumentation facility Neon Laboratory, Mumbai, India, for providing gift sample of drug.

Author contributions
SS performed the investigation, conducted the formal analysis, wrote the original draft, reviewed and edited the manuscript, conceptualized the study, designed the methodology, validated the results, and curated the data. VS and SKK contributed to the conceptualization of the study, designed the methodology, validated the results, conducted the investigation, performed the formal analysis, wrote the original draft, reviewed and edited the manuscript and supervised the project.

Funding
Authors acknowledges All India Council for Technical Education (AICTE) GPAT Fellowship for providing funding opportunity.

Availability of data and materials
The data that support the findings of this study are available from the corresponding author upon reasonable request.

Declarations

Ethics approval and consent to participate
The Committee for Control and Supervision of Experiments on Animals (CPCSEA/SN-10/RN-22/16-02-2020) under the guidance of the Ministry of Social Justice and Empowerment, Government of India, and based on the recommendations of the Institutional Animal Ethical Committee (IAEC) of Dr. H.S. Gour Vishwavidyalaya located in Sagar, Madhya Pradesh, India.

Consent for publication
All authors are agreeing for the publication of manuscript.

Competing of interests
The authors declare that they have no competing interests.

Author details
[1]Department of Pharmaceutical Sciences, Dr. Harisingh Gour Vishwavidyalaya, Sagar, Madhya Pradesh 470003, India. [2]Department of Zoology, Dr. Harisingh Gour Vishwavidyalaya, Sagar, Madhya Pradesh 470003, India. [3]Quality Assurance Laboratory, M.P. Council of Science and Technology, (Dept. of S&T, Govt. of M.P.), Bhopal, Madhya Pradesh, India.

Received: 26 December 2023 Accepted: 19 March 2024
Published online: 27 March 2024

References

1. Pillai SG, Johnson L, Bagde H (2023) Squamous cell carcinoma: a comprehensive review on causes, clinical presentation, diagnosis, prognosis, and prevention. J Nurs Res Patient Saf Pract 3(02):21–26
2. Souto EB, da Ana R, Vieira V, Fangueiro JF, Dias-Ferreira J, Cano A, Zielińska A, Silva AM, Staszewski R, Karczewski J (2022) Non-melanoma skin cancers: physio-pathology and role of lipid delivery systems in new chemotherapeutic treatments. Neoplasia 30:100810–100815
3. Adnan M, Akhter MH, Afzal O, Altamimi AS, Ahmad I, Alossaimi MA, Jaremko M, Emwas AH, Haider T, Haider MF (2023) Exploring nanocarriers as treatment modalities for skin cancer. Molecules 28(15):5905–5920
4. Srivastava S, Sharma D (2023) An approach to treat conundrum of skin cancer: bioactive loaded niosomes. Curr Drug Ther 18(4):342–349
5. Shah HS, Gotecha A, Jetha D, Rajput A, Bariya A, Panchal S, Butani S (2021) Gamma oryzanol niosomal gel for skin cancer: formulation and optimization using quality by design (QbD) approach. AAPS Open 7:1–5
6. Anand U, Dey A, Chandel AK, Sanyal R, Mishra A, Pandey DK, De Falco V, Upadhyay A, Kandimalla R, Chaudhary A, Dhanjal JK (2022) Cancer chemotherapy and beyond: current status, drug candidates, associated risks and progress in targeted therapeutics. Genes Dis 10(4):1367–1401
7. Kauslya A, Borawake PD, Shinde JV, Chavan RS (2021) Niosomes: a novel carrier drug delivery system. J Drug Deliv Ther 11(1):162–170
8. Mousazadeh N, Gharbavi M, Rashidzadeh H, Nosrati H, Danafar H, Johari B (2022) Anticancer evaluation of methotrexate and curcumin-coencapsulated niosomes against colorectal cancer cell lines. Nanomedicine 17(4):201–217
9. Abdelbary AA, AbouGhaly MH (2015) Design and optimization of topical methotrexate loaded niosomes for enhanced management of psoriasis: application of Box-Behnken design, in-vitro evaluation and in-vivo skin deposition study. Int J Pharm 485(1–2):235–243
10. Pandey M, Choudhury H, Gorain B, Tiong SQ, Wong GY, Chan KX, They X, Chieu WS (2021) Site-specific vesicular drug delivery system for skin cancer: a novel approach for targeting. Gels 7(4):218–255
11. Al-Mahallawi AM, Abdelbary AA, Aburahma MH (2015) Investigating the potential of employing bilosomes as a novel vesicular carrier for transdermal delivery of tenoxicam. Int J Pharm 485(1–2):329–340
12. Shah R, Bhattacharya S (2023) Preparation and physical characterization of Methotrexate encapsulated poly (n-methyl glycine) microspheres for the Rheumatoid arthritis treatment option. Results Chem 5:100875–100890
13. Paolino D, Cosco D, Muzzalupo R, Trapasso E, Picci N, Fresta M (2008) Innovative bola-surfactant niosomes as topical delivery systems of 5-fluorouracil for the treatment of skin cancer. Int J Pharm 353(1–2):233–242
14. Sezgin-Bayindir Z, Yuksel N (2012) Investigation of formulation variables and excipient interaction on the production of niosomes. AAPS PharmSciTech 13:826–835
15. Shewaiter MA, Selim AA, Rashed HM, Moustafa YM, Gad S (2023) Niosomal formulation of mefenamic acid for enhanced cancer targeting; preparation, characterization and biodistribution study using radiolabeling technique. J Cancer Res Clin Oncol 20:1–6
16. Shamma RN, Aburahma MH (2014) Follicular delivery of spironolactone via nanostructured lipid carriers for management of alopecia. Int J Nanomed 26:5449–5460
17. Hathout RM, Nasr M (2013) Transdermal delivery of betahistine hydrochloride using microemulsions: physical characterization, biophysical assessment, confocal imaging and permeation studies. Colloids Surf B 110:254–260
18. Hajizadeh MR, Maleki H, Barani M, Fahmidehkar MA, Mahmoodi M, Torkzadeh-Mahani M (2019) In vitro cytotoxicity assay of D-limonene niosomes: an

efficient nano-carrier for enhancing solubility of plant-extracted agents. Res Pharm Sci 14(5):448–458
19. Pourmoghadasiyan B, Tavakkoli F, Beram FM, Badmasti F, Mirzaie A, Kazempour R, Rahimi S, Larijani SF, Hejabi F, Sedaghatnia K (2022) Nanosized paclitaxel-loaded niosomes: formulation, in vitro cytotoxicity, and apoptosis gene expression in breast cancer cell lines. Mol Biol Rep 49(5):3597–3608
20. Ghumman SA, Ijaz A, Noreen S, Aslam A, Kausar R, Irfan A, Latif S, Shazly GA, Shah PA, Rana M, Aslam A, Altaf M, Kotwica-Mojzych K, Bin Jardan YA (2023) Formulation and characterization of curcumin niosomes: antioxidant and cytotoxicity studies. Pharmaceuticals (Basel) 16(10):1406–1420
21. Barani M, Reza Hajinezhad M, Sargazi S, Zeeshan M, Rahdar A, Pandey S, Khatami M, Zargari F (2021) Simulation, in vitro, and in vivo cytotoxicity assessments of methotrexate-loaded pH-responsive nanocarriers. Polymers 13(18):3153–3176
22. Moammeri A, Chegeni MM, Sahrayi H, Ghafelehbashi R, Memarzadeh F, Mansouri A, Akbarzadeh I, Abtahi MS, Hejabi F, Ren Q (2023) Current advances in niosomes applications for drug delivery and cancer treatment. Mater Today Bio. 23:100837. https://doi.org/10.1016/j.mtbio.2023.100837
23. Witika BA, Bassey KE, Demana PH, Siwe-Noundou X, Poka MS (2022) Current advances in specialised niosomal drug delivery: manufacture, characterization and drug delivery applications. Int J Mol Sci 23(17):9668–9677
24. Chen S, Hanning S, Falconer J, Locke M, Wen J (2019) Recent advances in non-ionic surfactant vesicles (niosomes): fabrication, characterization, pharmaceutical and cosmetic applications. Eur J Pharm Biopharm 144:18–39
25. Muzzalupo R, Tavano L (2015) Niosomal drug delivery for transdermal targeting: recent advances. Res Rep Transderm Drug Deliv 23–33
26. El-Far SW, Abo El-Enin HA, Abdou EM, Nafea OE, Abdelmonem R (2022) Targeting colorectal cancer cells with niosomes systems loaded with two anticancer drugs models; comparative in vitro and anticancer studies. Pharmaceuticals 15(7):816–829
27. Zaid Alkilani A, Hamed R, Abdo H, Swellmeen L, Basheer HA, Wahdan W, Abu Kwiak AD (2022) Formulation and evaluation of azithromycin-loaded niosomal gel: optimization, in vitro studies, rheological characterization, and cytotoxicity study. ACS Omega 7(44):39782–39793
28. Al-Mahallawi AM, Fares AR, Abd-Elsalam WH (2019) Enhanced permeation of methotrexate via loading into ultra-permeable niosomal vesicles: fabrication, statistical optimization, ex vivo studies, and in vivo skin deposition and tolerability. AAPS PharmSciTech 20:1–10
29. Demirbolat GM, Aktas E, Coskun GP, Erdogan O, Cevik O (2021) New approach to formulate methotrexate-loaded niosomes: in vitro characterization and cellular effectiveness. J Pharm Innov 1–6
30. Hnin HM, Stefánsson E, Loftsson T, Asasutjarit R, Charnvanich D, Jansook P (2022) Physicochemical and stability evaluation of topical niosomal encapsulating fosinopril/γ-cyclodextrin complex for ocular delivery. Pharmaceutics 14(6):1147–1155
31. Barot T, Rawtani D, Kulkarni P (2021) Development, characterization and in vitro–in vivo evaluation of Farnesol loaded niosomal gel for applications in oral candidiasis treatment. Heliyon 7(9):e07968
32. Verma A, Jain A, Tiwari A, Jain SK (2019) Preformulation considerations of Natamycin and development of Natamycin loaded niosomal formulation. Asian J Pharm Pharmacol 5(5):1022–1030
33. Zhang Y, Du X, Wang H, He Z, Liu H (2021) Sacubitril-Valsartan Cocrystal revisited: role of polymer excipients in the formulation. Expert Opin Drug Deliv 18(4):515–526
34. Li N, Qin Y, Dai D, Wang P, Shi M, Gao J, Yang J, Xiao W, Song P, Xu R (2022) Transdermal delivery of therapeutic compounds with nanotechnological approaches in psoriasis. Front Bioeng Biotechnol 9:804415–804430
35. Prabha J, Kumar M, Kumar D, Chopra S, Bhatia A (2024) Nano-platform strategies of herbal components for the management of rheumatoid arthritis: a review on the battle for next-generation formulations. Curr Drug Deliv 1–24
36. Mohamad Saimi NI, Salim N, Ahmad N, Abdulmalek E, Abdul Rahman MB (2021) Aerosolized niosome formulation containing gemcitabine and cisplatin for lung cancer treatment: optimization, characterization and in vitro evaluation. Pharmaceutics 13(1):59–72
37. Kulkarni P, Rawtani D, Barot T (2019) Formulation and optimization of long acting dual niosomes using box-Behnken experimental design method for combinative delivery of ethionamide and D-cycloserine in tuberculosis treatment. Colloids Surf A 565:131–142
38. Lala RR, Shinde AS (2021) Development, optimization, and in vitro evaluation of atorvastatin calcium and vinpocetine codelivery by solid lipid nanoparticles for cancer therapy. Future J Pharm Sci 7(1):1–4
39. Dallavalle S, Musso L, Cincinelli R, Darwiche N, Gervasoni S, Vistoli G, Guglielmi MB, La Porta I, Pizzulo M, Modica E, Prosperi F (2022) Antitumor activity of novel POLA1-HDAC11 dual inhibitors. Eur J Med Chem 228:113971–113982
40. Martins C, Rasbach E, Heppt MV, Singh P, Kulcsar Z, Holzgruber J, Chakraborty A, Mucciarone K, Kleffel S, Brandenburg A, Hoetzenecker W (2024) Tumor cell–intrinsic PD-1 promotes Merkel cell carcinoma growth by activating downstream mTOR-mitochondrial ROS signaling. Sci Adv 10(3):1–16
41. Bharadwaj R, Haloi J, Medhi S (2019) Topical delivery of methanolic root extract of *Annona reticulata* against skin cancer. S Afr J Bot 124:484–493
42. Ramana NV, Neelima R, Ratna KumarRao PKBV (2020) GC-MS profile, antibacterial, antifungal and anticancer activity of leaves and roots of *Vanda testacea* an epiphytic orchid. Int J Pharm Res 09752366:2377–2382
43. Sethiya A, Agarwal DK, Agarwal S (2020) Current trends in drug delivery system of curcumin and its therapeutic applications. Mini Rev Med Chem 20(13):1190–1232
44. Elmotasem H, Awad GE (2020) A stepwise optimization strategy to formulate in situ gelling formulations comprising fluconazole-hydroxypropyl-beta-cyclodextrin complex loaded niosomal vesicles and Eudragit nanoparticles for enhanced antifungal activity and prolonged ocular delivery. Asian J Pharm Sci 15(5):617–636
45. Sadarani B, Majumdar A, Paradkar S, Mathur A, Sachdev S, Mohanty B, Chaudhari P (2019) Enhanced skin permeation of Methotrexate from penetration enhancer containing vesicles: in vitro optimization and in vivo evaluation. Biomed Pharmacother 114:108770–108775
46. Abd El-Alim SH, Kassem AA, Basha M, Salama A (2019) Comparative study of liposomes, ethosomes and transfersomes as carriers for enhancing the transdermal delivery of diflunisal: in vitro and in vivo evaluation. Int J Pharm 563:293–303
47. Ramanunny AK, Wadhwa S, Singh SK, Kumar B, Gulati M, Kumar A, Almawash S, Al Saqr A, Gowthamarajan K, Dua K, Singh H (2022) Topical non-aqueous nanoemulsion of *Alpinia galanga* extract for effective treatment in psoriasis: in vitro and in vivo evaluation. Int J Pharm 624:121882–121899
48. Kaur N, Kaur M, Mahajan M, Jain SK (2020) Development, characterization and evaluation of nanocarrier based formulations of antipsoriatic drug "acitretin" for skin targeting. J Drug Deliv Sci Technol 60:102010–102015
49. Janakiraman K, Krishnaswami V, Sethuraman V, Rajendran V, Kandasamy R (2019) Development of methotrexate-loaded cubosomes with improved skin permeation for the topical treatment of rheumatoid arthritis. Appl Nanosci 1781–96
50. Asad MI, Khan D, Rehman AU, Elaissari A, Ahmed N (2021) Development and in vitro/in vivo evaluation of pH-sensitive polymeric nanoparticles loaded hydrogel for the management of psoriasis. Nanomaterials 11(12):3433–3459
51. Rajitha P, Shammika P, Aiswarya S, Gopikrishnan A, Jayakumar R, Sabitha M (2019) Chaulmoogra oil based methotrexate loaded topical nanoemulsion for the treatment of psoriasis. J Drug Deliv Sci Technol 49:463–476

Publisher's Note